

The first direct measurement of gravitational potential decay rate at cosmological scales and improved dark energy constraint

FUYU DONG,^{1,*} PENGJIE ZHANG,^{2,3,4,†} ZEYANG SUN,^{2,4} AND CHANGBOM PARK¹

¹*School of Physics, Korea Institute for Advanced Study (KIAS), 85 Hoegiro, Dongdaemun-gu, Seoul, 02455, Republic of Korea*

²*Department of Astronomy, School of Physics and Astronomy, Shanghai Jiao Tong University, Shanghai, 200240, China*

³*Division of Astronomy and Astrophysics, Tsung-Dao Lee Institute, Shanghai Jiao Tong University, Shanghai, 200240, China*

⁴*Key Laboratory for Particle Astrophysics and Cosmology (MOE)/Shanghai Key Laboratory for Particle Physics and Cosmology, China*

ABSTRACT

The integrated Sachs-Wolfe (ISW) effect probes the decay rate (DR) of large scale gravitational potential and therefore provides unique constraint on dark energy (DE). However its constraining power is degraded by the ISW measurement, which relies on cross-correlating with the large scale structure (LSS) and suffers from uncertainties in galaxy bias and matter clustering. In combination with lensing-LSS cross-correlation, DR can be isolated in a way free of uncertainties in galaxy bias and matter clustering. We applied this proposal to the combination of the DR8 galaxy catalogue of DESI imaging surveys and Planck cosmic microwave background (CMB) maps. We achieved the first DR measurement, with a total significance of 3.2σ . We verified the measurements at three redshift bins ($[0.2, 0.4]$, $[0.4, 0.6]$, $[0.6, 0.8]$), with two LSS tracers (the "low-density points" and the conventional galaxy positions). Despite its relatively low S/N, the addition of DR significantly improves dark energy constraints, over SDSS baryon acoustic oscillation (BAO) data alone or Pantheon supernovae (SN) compilation alone. For flat w CDM cosmology, the improvement in the precision of Ω_m is a factor of 1.8 over BAO and 1.5 over SN. For the DE equation of state w , the improvement factor is 1.3 over BAO and 1.4 over SN. These improvements demonstrate DR as a useful cosmological probe, and therefore we advocate its usage in future cosmological analysis.

Keywords: Cosmology: gravitational potential – Cosmology: cosmic background radiation – Cosmology: large-scale structure of Universe – Cosmology: gravitational lensing

1. INTRODUCTION

A variety of observable effects are induced by the interactions between CMB photons and the large-scale structure (LSS) that they cross along the line of sight (LOS), such as the integrated Sachs-Wolfe effect (ISW) effect (Sachs & Wolfe 1967) and CMB lensing (Zaldarriaga & Seljak 1998; Seljak & Zaldarriaga 1999; Hu 2000; Hu & Okamoto 2002; Lewis & Challinor 2006). The two are complementary in probing the gravitational potential ϕ of the universe. ISW probes the gravitational potential decay rate (DR) $\dot{\phi}$. In a flat universe obeying general relativity, $\dot{\phi} \neq 0$ at late-time only if dark energy exists. This makes it a unique probe of dark energy. Its detection is made possible through the ISW-LSS cross-correlation (Crittenden & Turok 1996; Seljak & Zaldarriaga 2000; Fosalba et al. 2003; Boughn & Crittenden 2004; Afshordi 2004; Afshordi et al. 2004; Fosalba & Gaztañaga 2004; Nolta et al. 2004; Boughn & Crittenden 2005; Padmanabhan et al. 2005; Corasaniti et al. 2005;

Vielva et al. 2006; McEwen et al. 2006; Cabré et al. 2007; Rassat et al. 2007; Raccañelli et al. 2008; Hernández-Monteagudo 2010; Massardi et al. 2010; Schiavon et al. 2012; Giannantonio et al. 2012; Planck Collaboration et al. 2014; Shajib & Wright 2016; Planck Collaboration et al. 2016a; Velten et al. 2018; Kovács et al. 2019; Bahr-Kalus et al. 2022). However, such measurement suffers from degeneracy between $\dot{\phi}$ and galaxy bias/matter clustering.

This degeneracy can be broken in a model independent way combining lensing-LSS cross-correlation measurement (Zhang 2006). Essentially, the ratio of two cross-correlations measures $\dot{\phi}/\phi$,¹ up to a prefactor depending on the geometry of the universe but free of galaxy bias and matter clustering. Furthermore, it is less sensitive to the survey masks, whose impacts on the cross-correlation measurements are largely canceled out

¹ For more general cases such as the case of modified gravity or dark energy with significant anisotropic stress, ϕ should be replaced with the lensing potential $\Phi_L \equiv (\phi - \psi)/2$. ϕ and ψ are defined through $d\tau^2 = (1 + 2\psi)dt^2 - (1 + 2\phi)\gamma_{ij}dx^i dx^j$ in the Conformal Newtonian Gauge.

* dongfy2020@kias.re.kr

† zhangpj@sjtu.edu.cn

in the ratio. In [Dong et al. \(2021a,b\)](#), we have measured both cross-correlations combining DESI imaging surveys and Planck maps. We explored two LSS tracers, namely the traditional galaxy positions, and low-density points (LDP) recently proposed by [Dong et al. \(2019\)](#). The ISW effect was detected at 3.2σ and the CMB lensing was detected at 56σ . Here we combine these measurements to determine the decay rate. Due to measurement errors, we can not simply take the ratio, otherwise the measured ratio will be biased. We have developed a unbiased estimator of measuring the ratio of two data sets. (Sun et al., in preparation) and will apply it here. There are also other studies that using the Planck CMB lensing map to help calibrate the bias of the sources in the ISW measurements, but in different ways ([Ferraro et al. 2015](#); [Planck Collaboration et al. 2016a](#)).

This paper is organized as follows. §2 introduces the methodology and data sets used in our analysis. §3 presents the measured decay rates at three redshifts. They significantly improve the dark energy constraint over existing baryon acoustic oscillation (BAO) or type Ia supernovae measurements. We discuss and conclude in §4. The estimator adopted to measure DR is briefly introduced in the Appendix A.

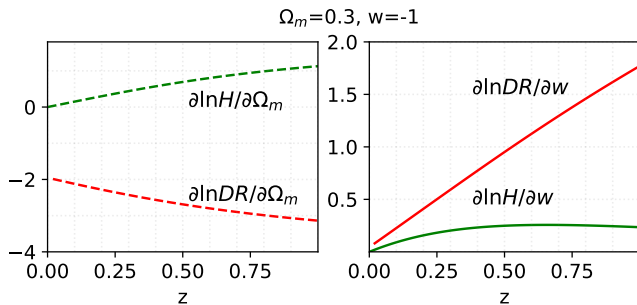


Figure 1. The sensitivities of DR to Ω_m and w , quantified by $\partial \ln DR / \partial \Omega_m$ (left panel) and $\partial \ln DR / \partial w$ (right panel). The results for $H(z)$ are plotted for comparison. For identical fractional measurement error, the constraint of Ω_m from DR will be a factor of 4 better than that from H on the median, and constraint of w from DR will be a factor of 7 better than that from H for $0 < z < 1$. A cosmology of $\Omega_m = 0.3$ and $w = -1$ is used for the plots.

2. METHODOLOGY AND DATA

2.1. Isolating the Decay Rate (DR) of Gravitational Potential

[Zhang \(2006\)](#) pointed out a proportionality relation between the ISW-LSS cross-power spectrum C_{I_g} and lensing-LSS cross-power spectrum $C_{\phi g}$,

$$C_{I_g}(\ell) \simeq DR(z_m) C_{\phi g}(\ell). \quad (1)$$

z_m is the mean redshift of a chosen galaxy redshift bin, namely galaxies located at $z_m - \Delta z/2 < z < z_m +$

Galaxy redshift	N_g	$DR(\text{LDP})$	$DR(\text{gal})$
$0.2 < z^P < 0.4$	1.33×10^6	0.094 ± 0.058	0.087 ± 0.054
$0.4 < z^P < 0.6$	1.66×10^6	0.180 ± 0.068	0.176 ± 0.065
$0.6 < z^P < 0.8$	1.54×10^6	0.057 ± 0.069	0.043 ± 0.068

Table 1. The galaxy samples selected from DESI imaging survey DR8 and the measured gravitational potential decay rate DR . We use both LDPs (low-density points) and galaxy positions as LSS tracers.

$\Delta z/2$. The coefficient DR is the decay rate that we can measure,

$$DR(z) = \left(-\frac{d \ln D_\phi}{d \ln a} \right) \left(\frac{aH(z)/c}{W_L(z)} \right). \quad (2)$$

This relations holds for both flat and curved universes. For brevity we focus on a flat universe hereafter. $H(z)$, a and c are the Hubble parameter at redshift z , the scale factor and the speed of light respectively. D_ϕ is the linear growth factor of gravitational potential ϕ ([Linder 2005](#)). Along with the onset of dark energy, ϕ decays with time. So in Eq. 2 we include explicitly a negative sign to make DR positive. Notice that DR defined above differs from the desired decay rate $d \ln D_\phi / d \ln a$ by factors in the last parenthesis, since lensing has an extra geometry dependence $W_L(z) = [1 - \chi(z)/\chi(z_s)]/\chi(z)$. $\chi(z) = \int cdz/H(z)$ is the comoving radial coordinate. For CMB lensing, the source redshift $z_s = 1100$. Fortunately, these extra factors do not depend on H_0 and thus avoid uncertainties in H_0 .

The above relation is expected to be valid for $z_m \gtrsim 0.2$ and $z_m > \Delta z$ ([Zhang 2006](#)). We numerically verify that it is accurate to 5% over the multipole range $\ell < 300$.² This is sufficiently precise given the $\sim 30\%$ measurement error in DR .

At redshifts where the ISW effect can be detected ($z \lesssim 1$), DR is determined by the matter density Ω_m and the dark energy equation of state w . Due to the intrinsic dependence of decay rate on $\dot{\phi}/\phi$, its sensitivity to w is a factor of $3/4/5$ higher at $z = 0.3/0.5/0.7$ than that of H (Fig. 1). This superior sensitivity also holds for Ω_m (Fig. 1). Later on we will find that such superior sensitivity partly compensates its significantly weaker measurement S/N, and leads to significant improvement in DE constraint over BAO and SNe Ia.

2.2. CMB Temperature Map and Lensing Map

In the following, we use C_{I_l} and $C_{\phi l}$ to represent the ISW-LDP cross-power spectrum and lensing-LDP cross-power spectrum. We use the Planck SMICA temperature product ([Planck Collaboration et al. 2016b](#)) for the

² The accuracy can be further improved when necessary. For example, we may replace z_m by the average redshift of galaxies.

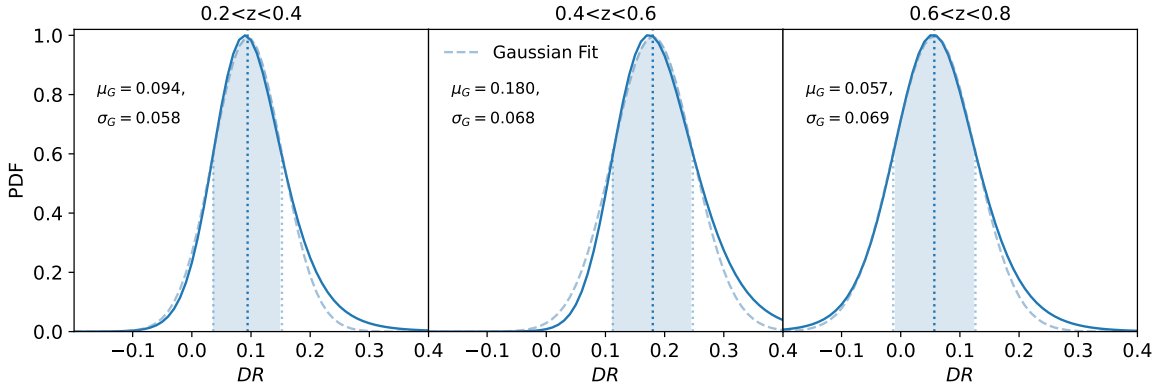


Figure 2. The probability distribution function of DR (blue solid line) obtained by the estimator of Eq. A1. It is well described by a Gaussian function (blue dashed line), for which we list the best-fitting values of the PDF. The PDF is normalized with its peak amplitude.

ISW-LDP cross-correlation measurement and the lensing product (Planck Collaboration et al. 2020) for the lensing potential-LDP cross-correlation measurement. For both products, the thermal Sunyaev-Zeldovich (tSZ) effect has been deprojected. The Planck temperature product is provided as a full-sky map, while the lensing product is provided as spherical harmonic coefficients a_{lm} of the lensing convergence in HEALPix FITS format (Górski et al. 2005) with $\ell_{max} = 4096$, for which we multiply them by a factor of $2/\ell/(\ell + 1)$ to produce the lensing potential.

To match the resolution of the LSS tracer density map, we downgrade the above CMB products to a lower resolution with $N_{side} = 512$. During the analysis, we adopt the Planck mask to remove pixels contaminated by Galactic dust or known point sources. Notice that to avoid systematic biases to the lensing data introduced by the mask effect, aliasing effect and reconstruction noise, we apply a tophat cut in multipole space for generating the lensing potential for which the details are introduced in Appendix B. The same filter is applied to the CMB temperature to eliminate its effect on the DR measurement.

2.3. Galaxy Catalogue and LDP Identification

For LSS tracers, we base on the photo- z galaxy catalog from the DESI Legacy Imaging Surveys. The DESI instrument is designed to measure the redshifts of galaxies and quasars from the northern hemisphere in a 14,000 deg^2 survey, for which the imaging data are provided by three projects: *the Beijing-Arizona Sky Survey* (BASS), *the Mayall z -band Legacy Survey* (MzLS), *the DECam Legacy Survey* (DECaLS). In combination with the *Dark Energy Survey* (DES), the joint sky coverage of the Data Release 8 (DR8) of the Legacy Surveys approaches $\sim 20000 \text{ deg}^2$, which is a key to reduce the statistical error in the ISW measurement. We select galaxies from

the DR8 photometric galaxy catalog³ and form volume-limited galaxy samples. The DR8 photometric catalog (Zou et al. 2019) is selected upon the three optical bands (g , r , z) and mid-infrared bands observed by the Wide-field Infrared Survey Explorer satellite (Zou et al. 2019; Silva et al. 2016; Flaugher 2005; Blum et al. 2016; Abbott et al. 2018). The photo- z of each galaxy is estimated by a local linear regression algorithm (Beck et al. 2016; Gao et al. 2018). The catalogue also provides apparent magnitudes in g , r , z bands, and stellar masses of galaxies.

LDPs depend on the galaxy sample selected. Following Dong et al. (2021a), we select galaxies with r -band absolute magnitudes⁴ $M_r < -21.5$ and $0.2 \leq z^P < 0.4$. This results into 1.33×10^6 galaxies. We exclude all regions within $R_s = 3'$ radius⁵ of any galaxies in this sample and define the remaining sky positions as LDPs. Statistically speaking, LDPs correspond to underdense regions (Dong et al. 2019, 2021a). We apply the same operations on galaxies at $0.4 < z^P < 0.6$ and $0.6 < z^P < 0.8$ respectively (Table 1).

We sample LDPs on equal-area HEALPix grids at $N_{side} = 4096$, which corresponds to an angular resolution of $0.859'$. We then follow Dong et al. (2021a) to define the pixelized LDP over-density field δ_{LDP} at $N_{side}=512$ resolution,

$$\delta_{LDP} = \frac{f_{LDP} - \bar{f}_{LDP}}{\bar{f}_{LDP}}. \quad (3)$$

³ http://batc.bao.ac.cn/~zouhu/doku.php?id=projects:desi_photoz;

⁴ The absolute magnitudes used have not been K-corrected. Since galaxies within the same photo- z bin have similar K-correction and the LDP generation is sensitive only to relative brightness between these galaxies, this lack of K-correction is not an issue for our purpose.

⁵ Larger R_s or more galaxies locates denser low density areas but less number of LDPs. The adopted $R_s = 3'$ is a balance between the two.

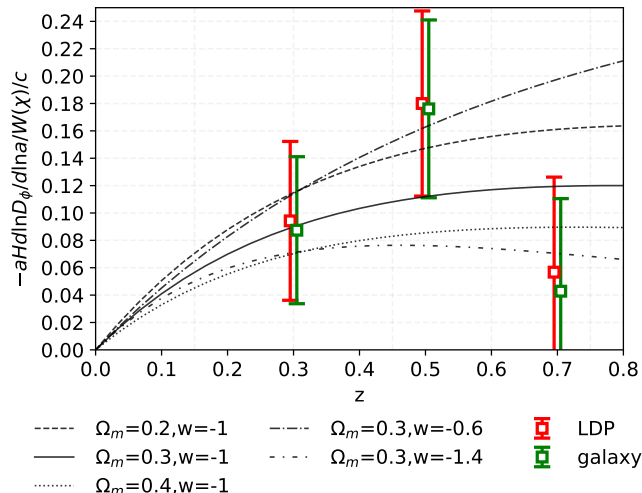


Figure 3. The gravitational potential decay rate DR measured at $0.2 < z < 0.4$, $0.4 < z < 0.6$ and $0.6 < z < 0.8$. Red(green) data points show the results obtained with LDPs(galaxies). Theoretical curves of five w CDM cosmologies are also shown for demonstration.

Here f_{LDP} is the fraction of each $N_{\text{side}} = 512$ pixel occupied by LDPs, and \bar{f}_{LDP} is the mean quantity averaged over the survey area. δ_{LDP} is tightly correlated with the matter overdensity δ_m and galaxy number overdensity δ_g , as we have verified in N-body simulations. The adopted magnitude cut, Δz , R_s and the definition of δ_{LDP} have yielded significant detection of the ISW-LDP cross-correlation (Dong et al. 2021a).

A combined mask from both galaxy catalogue⁶ and the Planck survey is applied to the LDP over-density field. Furthermore, to avoid possible foreground contaminations from the Galactic plane, we put an additional galactic mask with $|\text{DEC}| > 30^\circ$ to both the CMB maps and the LDP (galaxy) maps. We perform all the analysis in the Galactic coordinate system.

3. DR MEASUREMENTS AND IMPROVED DARK ENERGY CONSTRAINTS

3.1. Measurement of DR

The selection criterion in Section 2.3 results in a total number of $\sim 4.5 \times 10^6$ galaxies in three redshift bins ($[0.2, 0.4]$, $[0.4, 0.6]$ & $[0.6, 0.8]$, Table 1). We then follow the same procedure in Dong et al. (2021a,b) to measure the ISW-LDP cross-power spectrum $C_{\ell I}$ and the CMB lensing-LDP cross-power spectrum $C_{\phi I}$. Considering that $C_{\ell I}$ mainly arises from large angular scale

⁶ The survey mask is generated from the available random catalogues provided by the DR8 website, which contain the number of observation in the g, r, z bands and a general purpose artifact flag MASKBITS, according to the coordinates drawn from the observed distribution. We refer readers to Dong et al. (2021b) for the detailed procedure.

($\ell < 50$) while the measurement of $C_{\phi I}$ is noisy at $\ell < 10$, we choose $(\ell_{\text{min}}, \ell_{\text{max}}) \sim (9, 117)$ and six angular bins equally spaced in $\ln \ell$.

Instead of directly taking the ratio of these two cross-correlations, we use the likelihood method for estimating DR and the corresponding error bar (Appendix A). It directly evaluates $P(DR)$ using the exact analytical expression (Eq. A1). Since it involves no multi-parameter fitting, it is computationally fast. Furthermore, the resulting $P(DR)$ is unbiased and relies on no cosmological assumptions other than the proportionality relation. The obtained $P(DR)$ of three redshift bins are shown in Fig. 2. $P(DR)$ is very close to Gaussian. Therefore later we will adopt a Gaussian $P(DR)$ in cosmological parameter fitting.

The results of DR are shown in Table 1 & Fig.3. The detection significances of three redshifts are 1.62σ , 2.66σ and 0.82σ , respectively. The total significance is 3.2σ . For comparison, we also measure DR with the same set of galaxies used for generating LDPs, and obtain a total $\sim 3.2\sigma$ measurement. The measurements including the S/N are fully consistent with each other (Table.1). Because the sign of the cross-correlations of $C_{\ell I}$ and $C_{\phi I}$ is flipped for LDP, the sign of DR is identical to that measured with galaxies.

3.2. Constraint on a Flat w CDM Model

For the dark energy constraint, we restrict the analysis to the flat w CDM cosmology. To demonstrate its constraining power on DE, we show $DR(z)$ of various flat w CDM cosmology in Fig. 3. DR first increases with redshift ($DR \propto azH$) until $z \sim 1$, and then begins to decrease due to vanishing $\dot{\phi}$. A lower Ω_m or a less negative w leads to a higher DR . In particular, since $DR = 0$ if $\Omega_m = 1$, a non-zero measurement provides a smoking gun evidence of dark energy.

Nevertheless, the $\sim 3\sigma$ measurement of DR seems disappointing in constraining power in w . However, there are three points that boost its DE constraining power to be much stronger than that implied by the measurement S/N. We emphasize two here and postpone the third after the likelihood analysis. Firstly, as shown in Fig. 1, the sensitivity of DR to w and Ω_m is a factor of ~ 4 higher than that of H . Secondly, DR relies on fewer parameters than other data. For flat Λ CDM, it only relies on Ω_m . For flat w CDM, it relies on Ω_m and w . As comparisons, both BAO and SNe Ia depend on extra cosmological parameters such as H_0 (or r_s), and extra nuisance parameters in the data analysis.

Since $p(DR)$ is nearly Gaussian, we estimate the posterior distribution of (Ω_m, w) by $\mathcal{L} \propto \exp(-\chi^2/2)$ and

$$\chi^2 = \sum_{i=1}^3 \frac{(DR_{\text{obs}}(z_i) - DR_{\text{model}}(\Omega_m, w, z_i))^2}{\sigma_{DR}^2(z_i)}. \quad (4)$$

Here $\sigma_{DR}(z_i)$ is the corresponding error bar of the i -th DR measurement.

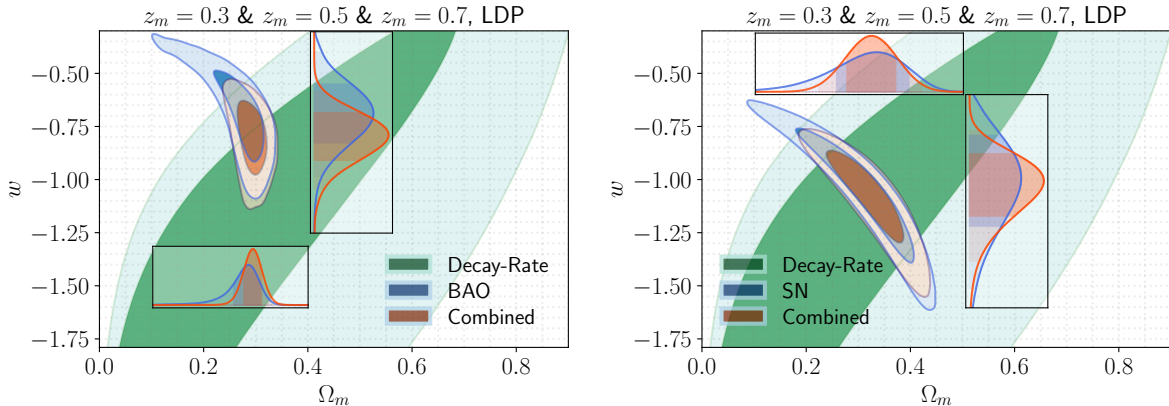


Figure 4. Constraints on the flat w CDM model, from BAO/DR/BAO+DR (left panel) and SN/DR/SN+DR (right panel). Partly due to the Ω_m - w degeneracy direction and partly due to its higher sensitivity on Ω_m and w , the inclusion of DR significantly improves over BAO or SN alone.

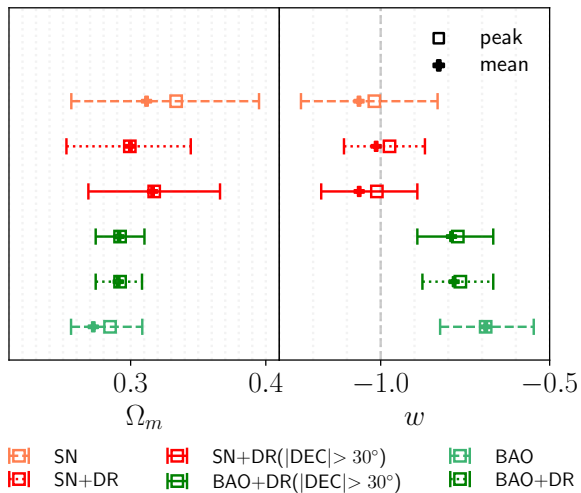


Figure 5. Improvement in w CDM constraints by including the DR measurement. “peak” refers to the best-fit value of the parameter and “mean” refers to the average value of the parameter. The improvement in parameter uncertainty is 1.4-2. $|\text{DEC} > 30^\circ|$ is an additional mask adopted to all maps used for deriving the main results in this paper (solid lines). We also show the results obtained without adopting this mask for comparison (dotted lines), which are consistent with the solid lines.

Fig.4 shows the constraints from DR measured by LDPs.⁷ Due to limited S/N, DR measurements alone suffer from a strong degeneracy between Ω_m and w . Since for a flat universe $\Omega_{\text{DE}} = 1 - \Omega_m$, the degeneracy direction just restates that higher dark energy density or less negative w (and therefore longer duration of dark energy dominance) results into higher DR. This behav-

ior is consistent with behaviors of theoretical curves in Fig. 3.

Nevertheless, Ω_m - w constraints from DR are still useful, since they are highly complementary to constraints from BAO and SNe Ia. Fig.4 shows the contours from SDSS BAO data (Alam et al. 2021),⁸ which includes observations of galaxy and quasar samples from the SDSS, BOSS, and the eBOSS surveys at $z < 2.2$ and Ly α forest observations over $2 < z < 3.5$ (Neveux et al. 2020; Hou et al. 2021; de Mattia et al. 2021; Tamone et al. 2020; Raichoor et al. 2021; Gil-Marín et al. 2020; Bautista et al. 2021). It also shows the contours from the Pantheon SNe Ia data (Scolnic et al. 2018). Clearly, the Ω_m - w degeneracy direction of DR is largely orthogonal to those of BAO and SN. The reason is that, for a flat universe both BAO and SN constrain Ω_m and w through their impacts on the same $H(z)$, although with different redshift weights. So the degeneracy direction is $\delta w \simeq c\delta\Omega_m$. $c \sim -(\partial H/\partial\Omega_m)/(\partial H/\partial w)_{z_*} = -[(1+z_*)^{-3w} - 1]/[3(1-\Omega_m)\ln(1+z_*)]$. z_* is the redshift where most constraining power locates. Therefore for both BAO and SN, $c_{\text{BAO}} < 0$ and $c_{\text{SN}} < 0$. In contrast, $c_{\text{DR}} > 0$ (Fig.1).

Therefore the inclusion of DR measurement significantly improves over BAO/SN constraints of Ω_m and w (Table 2 & Fig.5). Comparing to SDSS BAO alone, DR+BAO reduces σ_{Ω_m} (the statistical error in Ω_m) by a factor of 1.8 and σ_w by a factor of 1.29. For DR+SN, the factors are 1.45 & 1.42 respectively. We also find that the value of Ω_m estimated from BAO+DR ($0.294^{+0.018}_{-0.018}$) is more consistent with that of SN+DR ($0.317^{+0.049}_{-0.049}$) comparing to the case of BAO only ($0.285^{+0.024}_{-0.03}$) and SN ($0.334^{+0.061}_{-0.078}$) only. Another interesting finding is that the inclusion of DR alleviates the slight tension

⁷ Constraints with galaxy positions are very similar. Therefore we will not show them here.

⁸ We use the MCMC chains and likelihoods from the <https://www.sdss.org/science/cosmology-results-from-eboss>.

Table 2. Marginalized values and 68% confidence limits of (Ω_m, w) estimated from DR when in combination with different probes and with different choices of redshift.

		Ω_m (best-fit),	$\langle \Omega_m \rangle,$	$\sigma(\Omega_m)$	$w,$	$\langle w \rangle,$	$\sigma(w)$
	BAO	$0.285^{+0.024}_{-0.030},$	0.272,	0.035	$-0.682^{+0.13}_{-0.14},$	-0.69,	0.144
LDP($ \text{DEC} > 30^\circ$)	BAO+DR	$0.292^{+0.018}_{-0.018},$	0.291,	0.019	$-0.772^{+0.105}_{-0.120},$	-0.79,	0.118
LDP($ \text{DEC} > 30^\circ$)	BAO+DR (joint 3z)	$0.290^{+0.018}_{-0.018},$	0.289,	0.020	$-0.756^{+0.105}_{-0.120},$	-0.773,	0.119
LDP	BAO+DR	$0.292^{+0.016}_{-0.018},$	0.291,	0.019	$-0.764^{+0.097}_{-0.112},$	-0.783,	0.112
galaxy($ \text{DEC} > 30^\circ$)	BAO+DR	$0.294^{+0.016}_{-0.018},$	0.293,	0.019	$-0.787^{+0.105}_{-0.120},$	-0.807,	0.117
galaxy($ \text{DEC} > 30^\circ$)	BAO+DR (joint 3z)	$0.292^{+0.016}_{-0.018},$	0.292,	0.019	$-0.779^{+0.105}_{-0.120},$	-0.799,	0.118
galaxy	BAO+DR	$0.294^{+0.016}_{-0.018},$	0.293,	0.018	$-0.779^{+0.097}_{-0.120},$	-0.80,	0.112
	SN	$0.334^{+0.061}_{-0.078},$	0.312,	0.071	$-1.019^{+0.187}_{-0.217},$	-1.06,	0.21
LDP($ \text{DEC} > 30^\circ$)	SN+DR	$0.317^{+0.049}_{-0.049},$	0.316,	0.049	$-1.011^{+0.120}_{-0.164},$	-1.064,	0.148
LDP($ \text{DEC} > 30^\circ$)	SN+DR (joint 3z)	$0.310^{+0.051}_{-0.051},$	0.309,	0.051	$-0.996^{+0.120}_{-0.150},$	-1.042,	0.148
LDP	SN+DR	$0.299^{+0.045}_{-0.047},$	0.30,	0.046	$-0.974^{+0.105}_{-0.135},$	-1.013,	0.126
galaxy($ \text{DEC} > 30^\circ$)	SN+DR	$0.325^{+0.047}_{-0.047},$	0.323,	0.048	$-1.034^{+0.130}_{-0.165},$	-1.084,	0.149
galaxy($ \text{DEC} > 30^\circ$)	SN+DR (joint 3z)	$0.321^{+0.049}_{-0.047},$	0.321,	0.049	$-1.026^{+0.120}_{-0.165},$	-1.077,	0.150
galaxy	SN+DR	$0.307^{+0.045}_{-0.043},$	0.308,	0.045	$-0.996^{+0.105}_{-0.134},$	-1.037,	0.128

Note. — Columns for Ω_m , $\langle \Omega_m \rangle$ and $\sigma(\Omega_m)$ refers to the best-fit value of the matter density, the average value and the scatter with respect to $\langle \Omega_m \rangle$. Columns of w have the same meaning. We show the results obtained by adopting an additional galactic mask of $|\text{DEC}| > 30^\circ$ for measuring DR or not. The former result is more safe to use, while the latter shows smaller σ_w (especially for DR+SN). We also show the results obtained from a joint analysis of DR of three redshift slices for consistency check, labelled as ‘joint 3z’. These results are consistent with each other.

between w constrained from BAO/SN. Comparing to BAO, DR+BAO shift the bestfit w closer to -1 . As a cross-check, we also perform the analysis with DR measured from galaxy positions. The obtained constraints are consistent with LDP (Table 2).

4. DISCUSSION

We detect the gravitational potential decay rate (DR) in a model-independent way by combining the ISW-LSS cross-correlation with CMB lensing-LSS cross-correlation. The large overlap in survey region between DESI DR8 photo- z catalogue and Planck 2018 CMB data release enables us to detect DR at a total significance of 3.2σ within the redshift range of $0.2 < z < 0.8$. We demonstrate that DR highly complements BAO/SN, and therefore significantly improves their w CDM constraints.

In the above, we measure DR independently for each redshift. One may wonder whether a joint analysis of the cross-power spectrum from three redshift slices could improve the detection of DR, since non-zero cross-correlations are found between different redshifts, possibly caused by the same adopted mask, mixture of galaxies due to the photo- z error, as well as the wide ISW and CMB-lensing kernels. To do so, we consider the full covariance by including autocorrelations, $C_{II}(z_i) - C_{II}(z_i)$ ($C_{\phi l}(z_i) - C_{\phi l}(z_i)$), and cross-correlations, $C_{II}(z_i) - C_{II}(z_j)$ ($C_{\phi l}(z_i) - C_{\phi l}(z_j)$, $i \neq j$). We then fit values of DR of three redshifts simultaneously (Table 3). The cross-correlation between different redshifts is weak, so

Galaxy redshift	N_g	$DR(\text{LDP})$	$DR(\text{gal})$
$0.2 < z^P < 0.4$	1.33×10^6	0.111 ± 0.062	0.097 ± 0.056
$0.4 < z^P < 0.6$	1.66×10^6	0.177 ± 0.070	0.172 ± 0.067
$0.6 < z^P < 0.8$	1.54×10^6	0.068 ± 0.073	0.046 ± 0.070

Table 3. Similar to Table.1, but with DR obtained by taking into account of the cross-correlations between different redshifts.

it is expected that values of DR are consistent with the measured results from Table 1. Notice that there are only 300 noise FFP10 simulations (Planck Collaboration et al. 2020) available for estimating the full covariance matrix of CMB lensing. While the precision joint measurement of DR requires many more mocks. So the analysis here is just for consistency check.

As the ISW effect peaks around $z \sim 0.5$, our current measurements of DR focus on the low redshift ($0.2 < z < 0.8$). Considering that the optimistic S/N of the full-sky ISW signal for a standard Λ CDM model is around 7σ (Giannantonio et al. 2008), our detections of DR are already close to the statistical limit set by limited sky coverage and redshift range. However, it is necessary to include higher redshift in the future for the following reasons. First, more independent volumes are available for higher z , meaning lower statistical error. Second, the measurement of DR at high z , even a null detection, is useful for distinguishing between different

dark energy models. DESI, with over 30 million spectroscopic galaxy and quasar redshifts out to $z = 3.5$ and 14000 deg² sky coverage, will further improve the DR S/N, while reducing possible systematic errors in the current measurement (e.g. photometric redshift bias).

In addition to the DESI surveys in the northern sky, the *Large Synoptic Survey Telescope* (LSST, [LSST Dark Energy Science Collaboration \(2012\)](#)) under construction will cover about 18,000 deg² of the southern sky in the main survey for the next decade, with deeper image depths ($r \sim 24.5$). This will double the sky coverage of ISW/lensing-LSS cross-correlation measurement and improve DR measurement by another $\sim 40\%$.

At last, there are still other possibilities to further explore. For example, DR could also be detected through ISW-LSS cross-correlation + galaxy shear-LSS cross-correlation. Therefore, it can serve as a cross-check for

the DR measurement here and help eliminate possible systematics from each other.

ACKNOWLEDGMENTS

FD is supported by a KIAS Individual Grant PG079001 at Korea Institute for Advanced Study. CP is supported by a KIAS Individual Grant PG016904 at Korea Institute for Advanced Study. PZ and ZS are supported by National Science Foundation of China (11621303 & 11653003), the National Key R&D Program of China (2020YFC2201602), NO. CMS-CSST-2021-A02 and the 111 project. FD acknowledges the Korea Institute for Advanced Study for providing computing resources (KIAS Center for Advanced Computation) for this work. The authors thank the HEALPix/healpy software package ([Zonca et al. 2019](#); [Górski et al. 2005](#)).

REFERENCES

- Abbott, T. M. C., Abdalla, F. B., Allam, S., et al. 2018, *ApJS*, 239, 18, doi: [10.3847/1538-4365/aae9f0](#)
- Afshordi, N. 2004, *PhRvD*, 70, 083536, doi: [10.1103/PhysRevD.70.083536](#)
- Afshordi, N., Loh, Y.-S., & Strauss, M. A. 2004, *PhRvD*, 69, 083524, doi: [10.1103/PhysRevD.69.083524](#)
- Alam, S., Aubert, M., Avila, S., et al. 2021, *PhRvD*, 103, 083533, doi: [10.1103/PhysRevD.103.083533](#)
- Bahr-Kalus, B., Parkinson, D., Asorey, J., et al. 2022, *MNRAS*, doi: [10.1093/mnras/stac2040](#)
- Bautista, J. E., Paviot, R., Vargas Magaña, M., et al. 2021, *MNRAS*, 500, 736, doi: [10.1093/mnras/staa2800](#)
- Beck, R., Dobos, L., Budavári, T., Szalay, A. S., & Csabai, I. 2016, *MNRAS*, 460, 1371, doi: [10.1093/mnras/stw1009](#)
- Blum, R. D., Burleigh, K., Dey, A., et al. 2016, in *American Astronomical Society Meeting Abstracts*, Vol. 228, American Astronomical Society Meeting Abstracts #228, 317.01
- Boughn, S., & Crittenden, R. 2004, *Nature*, 427, 45, doi: [10.1038/nature02139](#)
- Boughn, S. P., & Crittenden, R. G. 2005, *NewAR*, 49, 75, doi: [10.1016/j.newar.2005.01.005](#)
- Cabré, A., Fosalba, P., Gaztañaga, E., & Manera, M. 2007, *MNRAS*, 381, 1347, doi: [10.1111/j.1365-2966.2007.12280.x](#)
- Corasaniti, P.-S., Giannantonio, T., & Melchiorri, A. 2005, *PhRvD*, 71, 123521, doi: [10.1103/PhysRevD.71.123521](#)
- Crittenden, R. G., & Turok, N. 1996, *PhRvL*, 76, 575, doi: [10.1103/PhysRevLett.76.575](#)
- de Mattia, A., Ruhlmann-Kleider, V., Raichoor, A., et al. 2021, *MNRAS*, 501, 5616, doi: [10.1093/mnras/staa3891](#)
- Dong, F., Yu, Y., Zhang, J., Yang, X., & Zhang, P. 2021a, *MNRAS*, 500, 3838, doi: [10.1093/mnras/staa3194](#)
- Dong, F., Zhang, P., Zhang, L., et al. 2021b, *ApJ*, 923, 153, doi: [10.3847/1538-4357/ac2d31](#)
- Dong, F., Zhang, J., Yu, Y., et al. 2019, *ApJ*, 874, 7, doi: [10.3847/1538-4357/ab0648](#)
- Ferraro, S., Sherwin, B. D., & Spergel, D. N. 2015, *PhRvD*, 91, 083533, doi: [10.1103/PhysRevD.91.083533](#)
- Flaugher, B. 2005, *International Journal of Modern Physics A*, 20, 3121, doi: [10.1142/S0217751X05025917](#)
- Fosalba, P., & Gaztañaga, E. 2004, *MNRAS*, 350, L37, doi: [10.1111/j.1365-2966.2004.07837.x](#)
- Fosalba, P., Gaztañaga, E., & Castander, F. J. 2003, *ApJL*, 597, L89, doi: [10.1086/379848](#)
- Gao, J., Zou, H., Zhou, X., & Kong, X. 2018, *ApJ*, 862, 12, doi: [10.3847/1538-4357/aacbc6](#)
- Giannantonio, T., Crittenden, R., Nichol, R., & Ross, A. J. 2012, *MNRAS*, 426, 2581, doi: [10.1111/j.1365-2966.2012.21896.x](#)
- Giannantonio, T., Scranton, R., Crittenden, R. G., et al. 2008, *PhRvD*, 77, 123520, doi: [10.1103/PhysRevD.77.123520](#)
- Gil-Marín, H., Bautista, J. E., Paviot, R., et al. 2020, *MNRAS*, 498, 2492, doi: [10.1093/mnras/staa2455](#)
- Górski, K. M., Hivon, E., Banday, A. J., et al. 2005, *ApJ*, 622, 759, doi: [10.1086/427976](#)
- Hernández-Monteaigudo, C. 2010, *A&A*, 520, A101, doi: [10.1051/0004-6361/200913344](#)
- Hou, J., Sánchez, A. G., Ross, A. J., et al. 2021, *MNRAS*, 500, 1201, doi: [10.1093/mnras/staa3234](#)
- Hu, W. 2000, *PhRvD*, 62, 043007, doi: [10.1103/PhysRevD.62.043007](#)

- Hu, W., & Okamoto, T. 2002, *ApJ*, 574, 566, doi: [10.1086/341110](https://doi.org/10.1086/341110)
- Kovács, A., Sánchez, C., García-Bellido, J., et al. 2019, *MNRAS*, 484, 5267, doi: [10.1093/mnras/stz341](https://doi.org/10.1093/mnras/stz341)
- Lewis, A., & Challinor, A. 2006, *PhR*, 429, 1, doi: [10.1016/j.physrep.2006.03.002](https://doi.org/10.1016/j.physrep.2006.03.002)
- Linder, E. V. 2005, *PhRvD*, 72, 043529, doi: [10.1103/PhysRevD.72.043529](https://doi.org/10.1103/PhysRevD.72.043529)
- LSST Dark Energy Science Collaboration. 2012, arXiv e-prints, arXiv:1211.0310. <https://arxiv.org/abs/1211.0310>
- Massardi, M., Bonaldi, A., Negrello, M., et al. 2010, *MNRAS*, 404, 532, doi: [10.1111/j.1365-2966.2010.16305.x](https://doi.org/10.1111/j.1365-2966.2010.16305.x)
- McEwen, J. D., Vielva, P., Hobson, M. P., Martínez-González, E., & Lasenby, A. N. 2006, arXiv e-prints, astro. <https://arxiv.org/abs/astro-ph/0602398>
- Neveux, R., Burtin, E., de Mattia, A., et al. 2020, *MNRAS*, 499, 210, doi: [10.1093/mnras/staa2780](https://doi.org/10.1093/mnras/staa2780)
- Nolta, M. R., Wright, E. L., Page, L., et al. 2004, *ApJ*, 608, 10, doi: [10.1086/386536](https://doi.org/10.1086/386536)
- Padmanabhan, N., Hirata, C. M., Seljak, U., et al. 2005, *PhRvD*, 72, 043525, doi: [10.1103/PhysRevD.72.043525](https://doi.org/10.1103/PhysRevD.72.043525)
- Planck Collaboration, Ade, P. A. R., Aghanim, N., et al. 2014, *A&A*, 571, A19, doi: [10.1051/0004-6361/201321526](https://doi.org/10.1051/0004-6361/201321526)
- . 2016a, *A&A*, 594, A21, doi: [10.1051/0004-6361/201525831](https://doi.org/10.1051/0004-6361/201525831)
- Planck Collaboration, Aghanim, N., Arnaud, M., et al. 2016b, *A&A*, 594, A11, doi: [10.1051/0004-6361/201526926](https://doi.org/10.1051/0004-6361/201526926)
- Planck Collaboration, Aghanim, N., Akrami, Y., et al. 2020, *A&A*, 641, A8, doi: [10.1051/0004-6361/201833886](https://doi.org/10.1051/0004-6361/201833886)
- Raccanelli, A., Bonaldi, A., Negrello, M., et al. 2008, *MNRAS*, 386, 2161, doi: [10.1111/j.1365-2966.2008.13189.x](https://doi.org/10.1111/j.1365-2966.2008.13189.x)
- Raichoor, A., de Mattia, A., Ross, A. J., et al. 2021, *MNRAS*, 500, 3254, doi: [10.1093/mnras/staa3336](https://doi.org/10.1093/mnras/staa3336)
- Rassat, A., Land, K., Lahav, O., & Abdalla, F. B. 2007, *MNRAS*, 377, 1085, doi: [10.1111/j.1365-2966.2007.11538.x](https://doi.org/10.1111/j.1365-2966.2007.11538.x)
- Sachs, R. K., & Wolfe, A. M. 1967, *ApJ*, 147, 73, doi: [10.1086/148982](https://doi.org/10.1086/148982)
- Schiavon, F., Finelli, F., Gruppuso, A., et al. 2012, *MNRAS*, 427, 3044, doi: [10.1111/j.1365-2966.2012.21974.x](https://doi.org/10.1111/j.1365-2966.2012.21974.x)
- Scolnic, D. M., Jones, D. O., Rest, A., et al. 2018, *ApJ*, 859, 101, doi: [10.3847/1538-4357/aab9bb](https://doi.org/10.3847/1538-4357/aab9bb)
- Seljak, U., & Zaldarriaga, M. 1999, *PhRvL*, 82, 2636, doi: [10.1103/PhysRevLett.82.2636](https://doi.org/10.1103/PhysRevLett.82.2636)
- . 2000, *ApJ*, 538, 57, doi: [10.1086/309098](https://doi.org/10.1086/309098)
- Shajib, A. J., & Wright, E. L. 2016, *The Astrophysical Journal*, 827, 116, doi: [10.3847/0004-637x/827/2/116](https://doi.org/10.3847/0004-637x/827/2/116)
- Silva, D. R., Blum, R. D., Allen, L., et al. 2016, in *American Astronomical Society Meeting Abstracts*, Vol. 228, American Astronomical Society Meeting Abstracts #228, 317.02
- Tamone, A., Raichoor, A., Zhao, C., et al. 2020, *MNRAS*, 499, 5527, doi: [10.1093/mnras/staa3050](https://doi.org/10.1093/mnras/staa3050)
- Velten, H., Fazolo, R. E., von Marttens, R., & Gomes, S. 2018, *Phys. Rev. D*, 97, 103514, doi: [10.1103/PhysRevD.97.103514](https://doi.org/10.1103/PhysRevD.97.103514)
- Vielva, P., Martínez-González, E., & Tucci, M. 2006, *MNRAS*, 365, 891, doi: [10.1111/j.1365-2966.2005.09764.x](https://doi.org/10.1111/j.1365-2966.2005.09764.x)
- Zaldarriaga, M., & Seljak, U. 1998, *PhRvD*, 58, 023003, doi: [10.1103/PhysRevD.58.023003](https://doi.org/10.1103/PhysRevD.58.023003)
- Zhang, P. 2006, *ApJ*, 647, 55, doi: [10.1086/505297](https://doi.org/10.1086/505297)
- Zonca, A., Singer, L., Lenz, D., et al. 2019, *Journal of Open Source Software*, 4, 1298, doi: [10.21105/joss.01298](https://doi.org/10.21105/joss.01298)
- Zou, H., Gao, J., Zhou, X., & Kong, X. 2019, *ApJS*, 242, 8, doi: [10.3847/1538-4365/ab1847](https://doi.org/10.3847/1538-4365/ab1847)

APPENDIX

A. AN ESTIMATOR TO MEASURE DR

If two data vectors ($\mathbf{d}_{1,2}$) are expected to obey $\mathbf{d}_2^{\text{theory}} = R\mathbf{d}_1^{\text{theory}}$, the ratio R can be estimated by Bayesian analysis. To be model independent, we take the parameters to be marginalized as $\lambda \equiv \mathbf{d}_1^{\text{theory}}$ and adopt a flat prior $P(\lambda)$. The marginalization can be done analytically and the the posterior distribution of R is given by

$$P(R|d_1, d_2) \propto \int P(d_1, d_2|R, \lambda)d\lambda \propto \det^{1/2}\mathbf{Q} \exp \left[\frac{1}{2} \left(\sum_i \mathbf{A}_i^T \mathbf{C}_i^{-1} \mathbf{d}_i \right)^T \mathbf{Q}^{-1} \left(\sum_i \mathbf{A}_i^T \mathbf{C}_i^{-1} \mathbf{d}_i \right)^T \right]. \quad (\text{A1})$$

Here $\mathbf{Q} = \sum_i \mathbf{A}_i^T \mathbf{C}_i^{-1} \mathbf{A}_i$, $\mathbf{A}_1 = \mathbf{I}$, $\mathbf{A}_2 = R\mathbf{I}$, and \mathbf{C}_i is the covariance matrix of \mathbf{d}_i . To measure DR by this estimator, we replace \mathbf{d}_1 and \mathbf{d}_2 with the CMB lensing-LSS cross-correlation $C_{\Phi l}(\ell)$ and the ISW-LSS cross-correlation $C_{II}(\ell)$. We use simulations to determine the covariance matrix. Noise Planck Full Focal Plane (FFP106) simulations (Planck Collaboration et al. 2020) are used to determine the mean-field bias and the covariance matrix estimation of $C_{\Phi l}(\ell)$ (Dong et al. 2021b). While for C_{II} , we simulate CMB temperature maps with the Planck cosmology to estimate the covariance matrix (Dong et al. 2021a). Fig.2 shows $P(DR)$. We then find the bestfit DR and σ_{DR} .

The estimator can be extended to more general cases of the theory-data mapping matrixes $\mathbf{A}_{1,2}$ and we refer readers to Sun et al. 2022 (in preparation) for details.

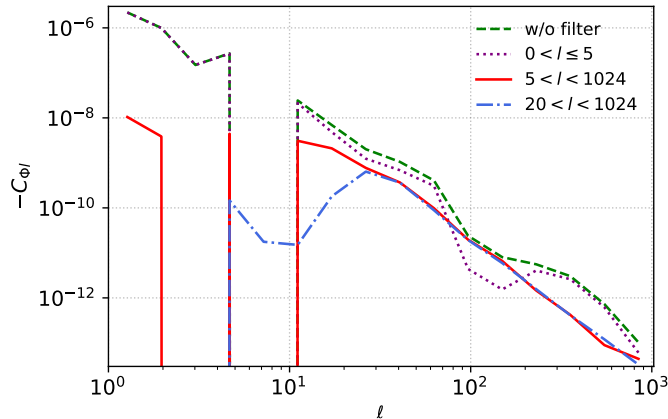


Figure 6. The lensing potential-LDP cross-correlation measured with different filters upon the masked CMB lensing potential. Green dashed line: without applying any filter to the lensing potential. Red solid line: applying a top hat filter of $5 < \ell < 1024$ to the lensing potential $\Phi_{\ell m}$. Purple dotted line: applying a top hat filter of $0 < \ell \leq 5$. Blue dashed-dotted line: applying a top hat filter of $20 < \ell < 1024$.

B. FILTERING THE CMB DATA

In this work, we produce the CMB lensing potential based on the Planck convergence product $\kappa_{\ell m}$: $\Phi_{\ell m} = 2/\ell/(\ell + 1)\kappa_{\ell m}$. However, the construction of $\kappa_{\ell m}$ in observation is contaminated with noise, which propagates onto $\Phi_{\ell m}$ and is amplified by a factor of $2/\ell/(\ell + 1)$. Therefore, there is a risk for directly using $\Phi_{\ell m}$, especially in the existence of mask. We find that our adopted mask is highly correlated with the lowest multipoles of $\Phi_{\ell m}$ ($\ell \leq 5$). Consequently, the contaminated cross power spectra at $\ell \leq 5$ are leaked onto higher ℓ and severely interferes our measurement of $C_{\phi l}$ at all scales. To avoid such effect, we adopt a tophat filter with $5 < \ell < 1024$ for generating the lensing potential map in this study. The result is shown in Fig.6, in which we have performed the scale cut test by varying the range of the tophat filter in multipole space: $\ell_{min} < \ell < \ell_{max}$. We find that $\ell_{min} = 5$ is a safe choice as the cross-power spectra of higher multipoles is almost identical to the one when adopting a larger ℓ_{min} . The choice of ℓ_{max} is to prevent the aliasing of high- ℓ noise power spectrum⁹.

⁹ In Dong et al. (2021b) we found that downgrading the lensing convergence map $\kappa_{\ell m}$ from its original resolution to a lower resolution one can introduce aliasing of high- ℓ noise power spectrum. An appropriate low-pass filter can prevent such effect. This effect is reduced to a low level when using $\Phi_{\ell m}$. However, we still keep this procedure for safety.